CAD of Waveguide Array Antennas Based on "Filter" Concepts

Huib J. Visser, *Member, IEEE,* and Marco Guglielmi, *Senior Member, IEEE*

***Abstract*—In this paper, an alternative approach for the design of open-ended waveguide array antennas is presented. The approach is based on microwave filter concepts. The exploitation of this alternative viewpoint has been made possible by the availability of a very efficient computer-aided design (CAD) tool which is based on a full-wave modal analysis technique. In this paper, we first outline the technique for the efficient analysis of open-ended waveguide array antennas. Using the software developed and following the alternative design approach, two different application examples are then shown, indicating how the alternative viewpoint introduced gives indeed significant additional degrees of freedom.**

***Index Terms*— Antenna arrays.**

I. Introduction

THE demand for increased sophistication and decreased development effort for phased-array antennas, motivates the continuous development of new computationally efficient computer-aided design (CAD) tools. In this paper, we present an accurate and computationally efficient full-wave theory that can be used to study and design open-ended waveguide array antennas. The increased computational efficiency achieved opens up the possibility of exploring new viewpoints in the design of such antennas as clearly demonstrated by two applications discussed in Section V.

Phased-array antennas generally consist of a large number of identical radiators arranged into a periodic lattice. The infinitely periodic structure is therefore a convenient starting point for the antenna design. To study an infinitely periodic structure, we only need to analyze one "unit cell" element, which consists, in its most basic form, of the transition from a cylindrical waveguide to the free-space unit cell [1]–[3]. In the free-space unit cell, the electromagnetic fields can be decomposed into Floquet modes so that the unit cell is, in fact, equivalent to a cylindrical waveguide with phase-shift walls. The study of the infinite array problem is therefore reduced to a waveguide discontinuity problem, namely the transition from a metallic waveguide to a phase-shift wall waveguide.

The design of modern microwave components generally requires full-wave analysis techniques in order to accurately account for all higher order mode interactions. A popular procedure which is frequently used in the context of waveguide discontinuity problems is the scattering matrix formulation of the mode-matching procedure [4]. This approach has also been used in the analysis of open-ended waveguide phased-array antennas [5]–[7]. The resulting codes, however, although accurate, can be computationally very inefficient. In addition, mode matching can be affected by "relative convergence" problems [8], potentially giving rise to erroneous solutions. Recently, a multimode equivalent network representation for arbitrary planar waveguide junctions has been developed in terms of multimode admittance or impedance parameters [9]. This technique was originally developed in the context of CAD tools for microwave filters and is extended here to the efficient analysis of waveguide-to-free-space unit cell junctions.

It is important to note that both the mode-matching method and the multimode equivalent network representation method belong to the family of modal analysis, but there are substantial differences. In applying a mode-matching procedure to the analysis of a waveguide junction, the unknown fields are expanded in infinite sets of normal modes [5]–[7]. Then the continuity of tangential electric and magnetic fields at the discontinuity is enforced. The resulting equations are rewritten into a set of equations involving unknown coefficients only. The series are then simultaneously truncated and the system is solved. The fact that infinite series are truncated simultaneously can give rise to "relative convergence" problems. Furthermore, in the scattering formulation of the mode-matching procedure, a frequency dependent matrix inversion is required for the characterization of every discontinuity [6], [7]. Then, in order to characterize cascaded discontinuities, an additional frequency dependent matrix inversion is required for every cascading operation [6], [7]. As we will see, using the method of the multimode equivalent network representation, no matrix inversions are required to characterize a discontinuity and, in order to characterize cascaded discontinuities, only one matrix inverse operation is required. Furthermore, because of its specific formulation, the method is uniformly convergent, thus not susceptible to "relative convergence" problems.

In this paper, we first describe in detail the development of the multimode admittance network formulation as well as additional means to further improve the computational efficiency. We then compare the results obtained with our theory with both measured and simulated results. Then, an alternative design procedure for infinite open-ended waveguide phased-array antennas is presented. The alternative procedure essentially consists of viewing the array as a microwave filter with the feeding waveguide as the input port and with free-space as the output port. Two specific design examples are

Manuscript received June 4, 1997; revised June 1, 1998. This work was supported in part by the Royal Netherlands Navy.

H. J. Visser is with TNO Physics and Electronics Laboratory, The Hague, 2509JG The Netherlands.

M. Guglielmi is with the European Space Research and Technology Centre, Noordwijk, 2201AZ, The Netherlands.

Publisher Item Identifier S 0018-926X(99)04432-4.

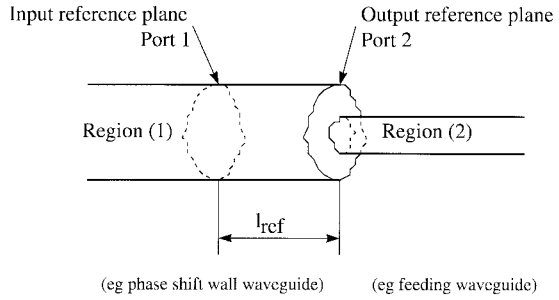

Fig. 1. Planar junction between two arbitrary waveguides.

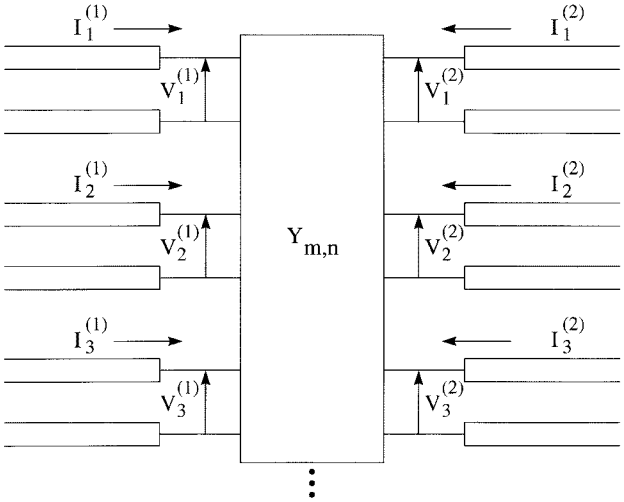

Fig. 2. Multimode equivalent network representation of the junction shown in Fig. 1.

finally discussed indicating how the new approach presented indeed gives significant additional degrees of freedom.

II. The Basic Admittance Formulation

The structure to be analyzed is a planar junction between two arbitrary waveguides, as shown in Fig. 1. The two waveguides could be, for instance, the feeding rectangular waveguide of the array and the phase-shift wall waveguide, as already discussed. The objective of this section is to discuss a method for the development of the multimode equivalent network representation for the junction in the form shown in Fig. 2. The key feature of the method described is that it starts from the wanted final results, the equivalent network representation, in order to obtain analytical expressions for the evaluation of the relevant matrix elements. The procedure is based on general network theory and is equivalent to ideally *measuring directly* the value of the admittance parameters.

In mathematical terms, the network in Fig. 2 is equivalent to the following linear system:

$$I_m^{(\delta)} = \sum_{n=1}^{\infty} Y_{m,n}^{(\delta,1)}.V_n^{(1)} + \sum_{n=1}^{\infty} Y_{m,n}^{(\delta,2)}.V_n^{(2)} \qquad (1)$$

where $I_m^{(\delta)}$ and $V_n^{(\delta)}$ are modal currents and voltages, respectively, and where δ can be 1 for region (1) or 2 for region (2), as shown in Fig. 1. The modal currents and voltages in

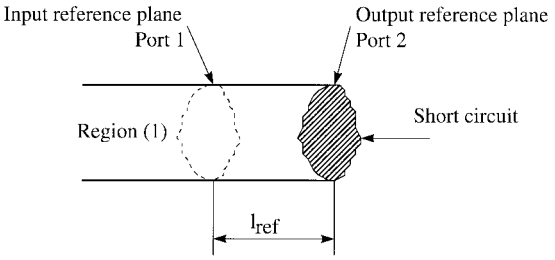

Fig. 3. Structure used for the evaluation of the $Y_{m,n}^{(1,1)}$ and $Y_{m,n}^{(2,1)}$ elements. A short circuit is placed at port 2 of Fig. 1 and the distance l_{ref} is introduced between in and output ports.

(1) are the amplitudes of the vector mode functions $\mathbf{h}_m^{(\delta)}$ and $\mathbf{e}_m^{(\delta)}$ relevant to the waveguide cross section (δ). The vector mode functions for standard cylindrical waveguides can be found in [10], the vector mode functions for a phase-shift wall waveguide are derived in the Appendix.

The system in (1) can now be used to actually obtain *directly* a formal expression for the evaluation of the $Y_{m,n}$ elements. We can, in fact, write

$$Y_{m,n}^{(\delta,\gamma)} = \frac{I_m^{(\delta)}}{V_n^{(\gamma)}}; \quad \forall V_i^{(\xi)} = 0,\ i \neq n,\ \xi \neq \gamma \qquad (2)$$

where γ and ξ can be 1 for region (1) or 2 for region (2), respectively. The expression in (2) can now be rewritten in the form

$$Y_{m,n}^{(\delta,\gamma)} = \frac{\int_{\mathrm{CS}(\delta)} \mathbf{H}^{(\delta)}[V_n^{(\gamma)}].\mathbf{h}_m^{(\delta)}\, ds'}{V_n^{(\gamma)}} \qquad (3)$$

where $\mathbf{H}^{(\delta)}[V_n^{(\gamma)}]$ is the TM field generated at port (δ) by the incident mode of amplitude $V_n^{(\gamma)}$ in port (γ). CS(δ) is the cross section (δ).

To explain the use of (2) and (3), we can start with the admittance elements $Y_{m,n}^{(1,1)}$. For these elements, the definition requires a single-mode incident from the left (port 1) and a short circuit in port 2. The distance l_{ref} must now be introduced between the input and output ports since we can not measure a voltage on a short circuit. The resulting structure becomes the one shown in Fig. 3 for which we can write directly

$$Y_{m,n}^{(1,1)} = -j.Y_{0m}^{(1)}.\cot(\beta_m^{(1)} l_{\mathrm{ref}}).\delta_{m,n} \qquad (4)$$

where $\delta_{m,n}$ is the Kronecker delta (equal to one for $m = n$; equal to zero otherwise).

For the elements $Y_{m,n}^{(2,1)}$, the definition in (2) requires again a single-mode incident from the left (port 1) and a short circuit in port 2. The current response will now be measured at port 2 using standard orthogonality [10] and the same structure in Fig. 3. Using then simple transmission line calculations, the resulting expression is

$$Y_{m,n}^{(2,1)} = -j.\frac{Y_{0m}^{(1)}}{\sin(\beta_m^{(1)} l_{ref})}\langle \mathbf{h}_m^{(1)}, \mathbf{h}_n^{(2)^*} \rangle \qquad (5)$$

which can also be used for $Y_{m,n}^{(1,2)}$ since the junction is lossless and reciprocal. Finally, for the elements $Y_{m,n}^{(2,2)}$, the definition

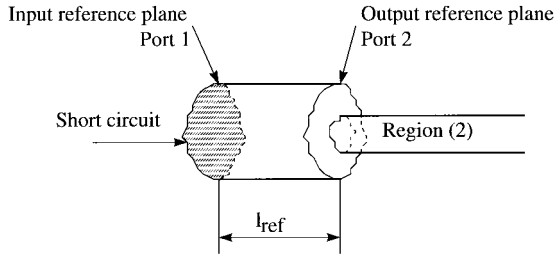

Fig. 4. Structure used for the evaluation of the $Y_{m,n}^{(2,2)}$ elements. A short circuit is placed at port 1 of Fig. 1.

in (2) requires a single mode exciting from the right (port 2) and a short circuit at port 1. The situation is now as indicated in Fig. 4 and the current response is again taken at port 2. To use (3), we now need to write an expression for $\mathbf{H}^{(2)}$. Taking into account the continuity of the TM field at port (2), we can write

$$\mathbf{H}^{(2)} = \sum_{k=1}^{\infty} I_k^{(1)} \mathbf{h}_k^{(1)} = \sum_{k=1}^{\infty} -j.Y_{0k}^{(1)} \cot(\beta_k^{(1)} l_{\text{ref}}) V_k^{(1)} \mathbf{h}_k^{(1)}. \tag{6}$$

Using again the orthogonality of the modes and simple transmission line theory, we then obtain

$$Y_{m,n}^{(2,2)} = \sum_{k=1}^{\infty} -j.Y_{0k}^{(1)} \cot(\beta_k^{(1)} l_{\text{ref}}) \langle \mathbf{e}_k^{(1)}, \mathbf{e}_n^{(2)^*} \rangle \langle \mathbf{h}_k^{(1)}, \mathbf{h}_m^{(2)^*} \rangle. \tag{7}$$

In all of the expressions derived, the symbol $\langle\ \rangle$ stands for the scalar product of the quantities involved (coupling integrals resulting from the use of the orthogonality conditions) and $\mathbf{e}$ and $\mathbf{h}$ are the normalized vector mode functions of the waveguides in the appropriate regions. $\beta_m^{(1)}$ is the propagation constant of the modes in region (1) and $Y_{0m}^{(1)}$ is the corresponding characteristic admittance. $*$ denotes the complex conjugate.

It is important to note that only the calculation of the $Y_{m,n}^{(2,2)}$ elements require summations and that the running index of the summations affect only the modes of the larger waveguide, namely region (1). Furthermore, the indexes m and n represent TE and TM modes at port (1) and (2) of the multimode equivalent network representation, while k represents TE and TM modes in region (1). In all summations, TE and TM modes are sorted according to their increasing cutoff wave number. The energy stored in the discontinuity is correctly accounted for once the $Y_{m,n}^{(2,2)}$ summations reach numerical convergence.

When the admittance coupling matrices of individual discontinuities have been obtained, cascaded discontinuities can be easily analyzed by constructing a global multimode equivalent network representation. An important feature of this method is that the analysis of the global network thus obtained requires only one inversion per frequency point (or angle) of a banded linear system and can therefore be performed very efficiently [11]. The dimension of this system is determined by the accuracy required in the final solution. The separate control over the required accuracy from the one over the stored energy [$Y_{m,n}^{(2,2)}$ summations] ensure uniform convergence of the results and thus eliminates "relative convergence" problems. The summations involved however, can be treated in order to significantly further increase the computational efficiency.

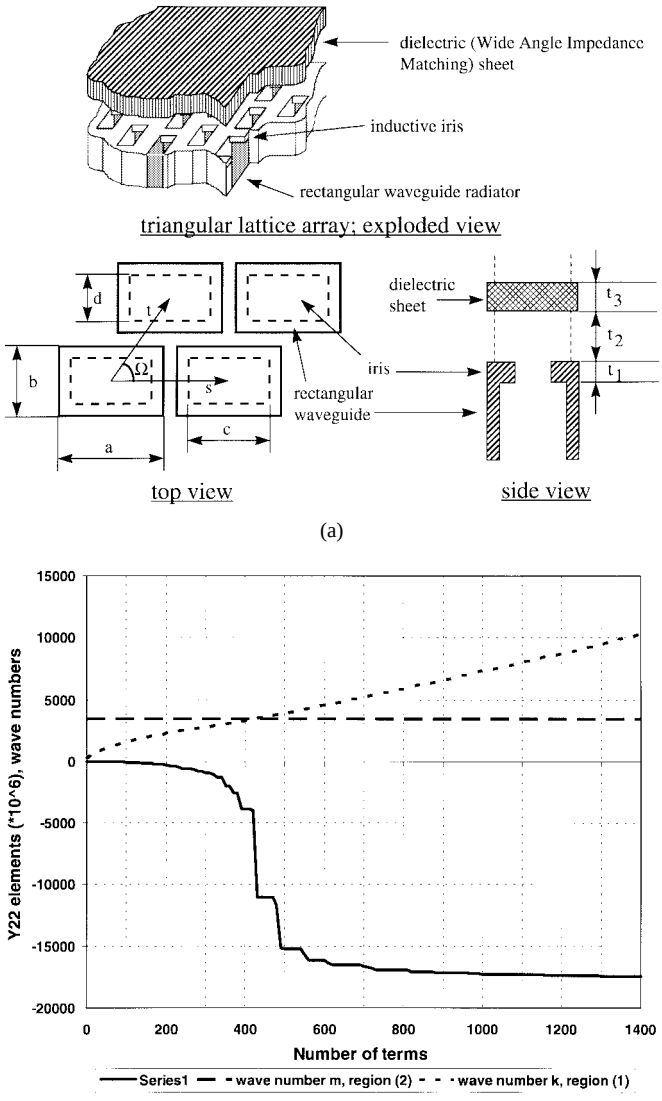

Fig. 5. Evolution of $Y_{m,n}^{(2,2)}$ as function of the summing index for a rectangular waveguide to free-space junction in an infinite waveguide array antenna. (a) Array configuration. (b) $(m, n) = (40, 40)$.

III. Improving Computational Efficiency

In order to investigate the behavior of $Y_{m,n}^{(2,2)}$ as function of the summing index k, we analyze an infinite rectangular waveguide array antenna as shown in Fig. 5(a). The array lattice is triangular, an inductive iris is placed into every waveguide aperture, and a dielectric sheet is placed in front of the antenna aperture for wide-angle impedance-matching purposes [5]. Fig. 5(b) shows a typical example of the evolution of $Y_{m,n}^{(2,2)}$ for the waveguide to free-space unit cell junction of the structure as function of k, for a given set of (m, n). As we increase the maximum number of terms in the summation of (7), we can see that there are distinct areas of running index k where the main contribution to $Y_{m,n}^{(2,2)}$ can

be found. Rather than starting the summation at $k = 1$ and proceed till convergence is reached, we would like to start the summation at the centers of main contribution and proceed in both directions till convergence is reached. To do so, we need to find a way to pinpoint the starting points of the summations. In the same figure, we also show the eigenvalue associated with mode m and mode n ($m = n$ for this particular example) and the value of the eigenvalue associated with summing index k. The figure shows that the main contribution can be found where the eigenvalues coincide, a result in correspondence with intuition. By using a linear interpolation, we can easily determine the appropriate starting points for the summation in k, i.e., the centers of the areas of strong contribution, thus strongly improving the computational efficiency.

Another method to improve the computational efficiency is to reduce the frequency dependent computations. To this end, we can add and subtract to (7) a *static* series [12], defined as

$$\overline{Y}_{m,n}^{(2,2)} = \sum_{k=1}^{\infty} -j.\overline{Y}_{0k}^{(1)} \cot(\overline{\beta}_k^{(1)} l_{\text{ref}}) \overline{\langle \mathbf{e}_k^{(1)}, \mathbf{e}_n^{(2)^*} \rangle \langle \mathbf{h}_k^{(1)}, \mathbf{h}_m^{(2)^*} \rangle} \tag{8}$$

obtaining for the $Y_{m,n}^{(2,2)}$ elements the following expression

$$Y_{m,n}^{(2,2)} = \overline{Y}_{m,n}^{(2,2)} - \tilde{Y}_{m,n}^{(2,2)} \tag{9}$$

where the second term in the right-hand side of (9) (called the *dynamic* series) is given by

$$\begin{aligned} \tilde{Y}_{m,n}^{(2,2)} &= \sum_{k=1}^{\infty} \Big\{ -j.\overline{Y}_{0k}^{(1)} \cot(\overline{\beta}_k^{(1)} l_{\text{ref}}) \overline{\langle \mathbf{e}_k^{(1)}, \mathbf{e}_n^{(2)^*} \rangle \langle \mathbf{h}_k^{(1)}, \mathbf{h}_m^{(2)^*} \rangle} \\ &\quad + j.Y_{0k}^{(1)} \cot(\beta_k^{(1)} l_{\text{ref}}) \langle \mathbf{e}_k^{(1)}, \mathbf{e}_n^{(2)^*} \rangle \langle \mathbf{h}_k^{(1)}, \mathbf{h}_m^{(2)^*} \rangle \Big\} \end{aligned} \tag{10}$$

and where the bars denote static quantities obtained by letting the frequency go to zero in the original expressions.

Following this formulation, the static term in (8) needs to be calculated only once before starting the frequency or angle loop. The convergence of the dynamic sum is now much faster due to the fact that the summation term in (10) tends to zero for large values of the running index k.

IV. Numerical Validation

Fig. 6 shows the computed reflection coefficient in the diagonal plane for the embedded element of the structure in Fig. 5(a), obtained using the admittance formulation (from now on called the direct method) and as calculated using a mode-matching procedure. Inspection of the embedded element reflection coefficient shows that for this array antenna a "blind scan angle" occurs at 53° from broadside, meaning that when used as a *phased*-array antenna at a scan angle of 53° from broadside in the diagonal plane, all the energy will be reflected. For operation within a scan cone of 45° the reflection is "reasonably" low; the corresponding VSWR is less than 2 : 1. Very good agreement can be observed, proving that the same accuracy can be obtained by both methods. The direct method, however, is computationally more efficient and is not susceptible to "relative convergence" problems.

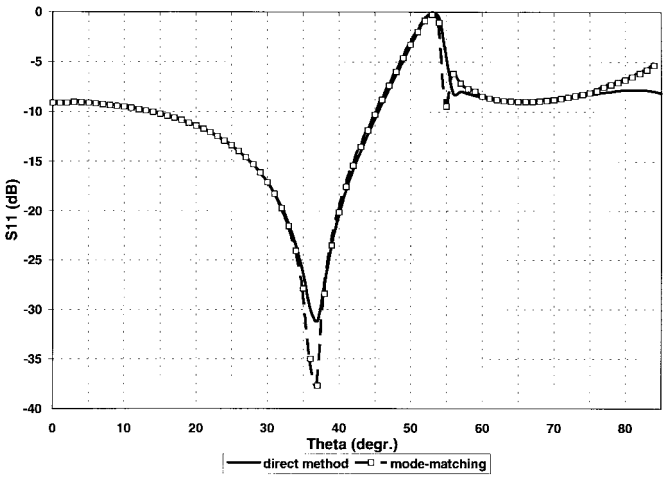

Fig. 6. Reflection coefficient in the diagonal plane for the array antenna shown in Fig. 5(a). $a/b = 4.14$, $c/d = 2.98$, $s/t = 1.73$, $t_1/t_2 = 0.4$, $t_1/t_3 = 0.91$, $a/\lambda_0 = 0.84$.

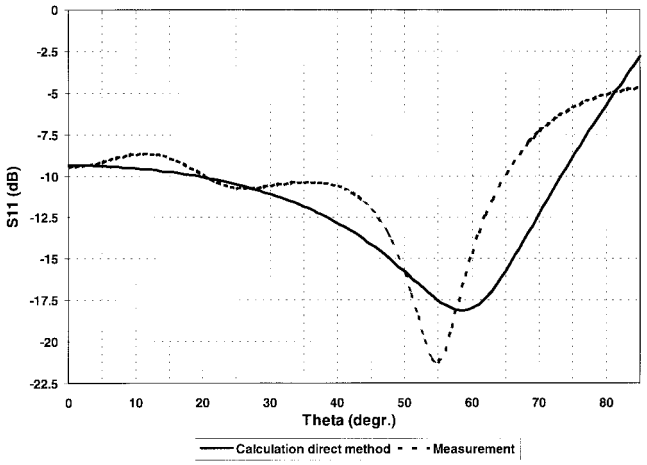

Fig. 7. Calculated E-plane reflection coefficient for the infinite array shown in Fig. 5(a) with irises and dielectric sheet removed ($t_1 = t_2 = t_3 = 0$). The measured reflection coefficient for a *finite* 175-elements array antenna is also shown.

To give an idea of the typical central processing unit (CPU) time improvement, the use of the techniques described produces an increase of speed over the basic direct method by nearly a factor 3 for the structure in Fig. 5(a) (21.8 s per point, using an IBM RISC 6000 platform). The same structure was also analyzed with standard mode matching [13]. The direct method is about an order of magnitude faster.

In Fig. 7 we show the results obtained from a simulation using the direct method for an infinite array and the measurements performed on a finite 175-element array. The array is the same as the one used in the calculations of Fig. 6, but now with the irises and the dielectric sheet removed. The reflection coefficient in the E plane is shown. In this plane no "blind scan angles occur." In the measurements we see a periodic variation of the reflection coefficient. This effect is due to the finiteness of the array. We do see, however, that the measured values follow the simulated ones. Taking into consideration

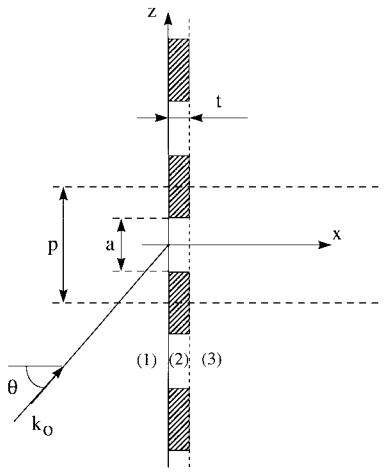

Fig. 8. Infinite thick grating.

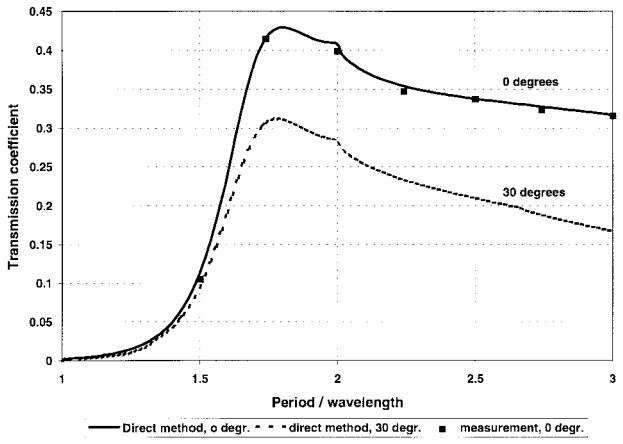

Fig. 9. Normalized transmission coefficient versus the relative period p/λ for the thick grating shown in Fig. 8 with $a/p = 1/3$, $t/p = 1/3$ and for two angles of incidence $\theta = 0°$ and $\theta = 30°$. The crosses are computed in [13] with $\theta = 0°$.

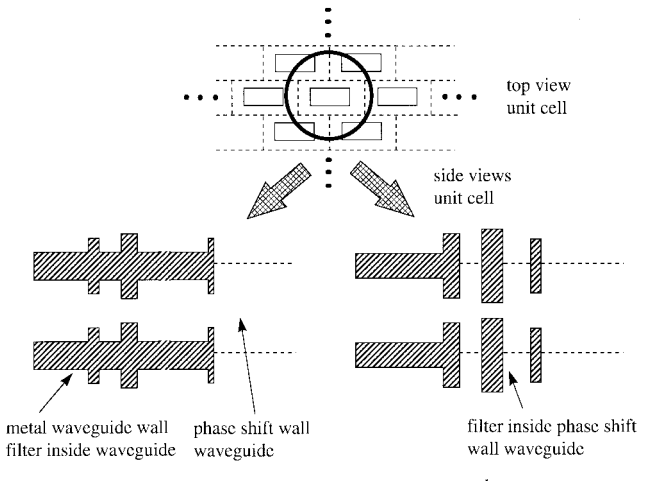

Fig. 10. Novel open-ended waveguide array antenna concepts. (a) Infinite planar array with filtering structure inside the rectangular waveguides. (b) Infinite planar array with filtering structure in the phase-shift waveguides.

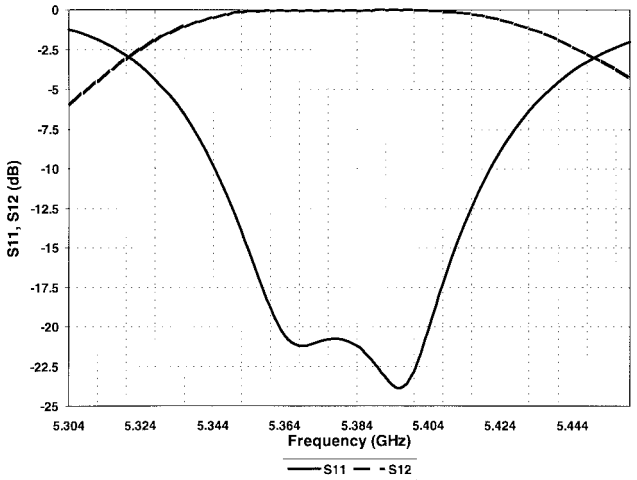

Fig. 11. Frequency response of the embedded element in the array antenna of Fig. 10(a).

that we compare infinite array calculations and small size finite-array measurements, the agreement between calculations and measurements is very reasonable. The agreement between calculations and measurements will improve with increasing number of array elements.

As a further validation, we analyze the transmission coefficient for the thick grating (shown in Fig. 8) for two angles of incidence. The results are shown in Fig. 9 and coincide exactly with earlier published results [14], [15].

V. "Filter" Design of Waveguide Phased-Array Antennas

Having described the analysis technique and having shown the accuracy of the CAD tool developed, we now discuss an alternative design procedure for open-ended waveguide phased-array antennas. The basic concept is to view the unit cell of the infinite array as a filter structure. In other words, we consider the input feeding waveguide as the input port and the phase shift wall waveguide as the output port. The objective of the design is to obtain a phased-array antenna with a prescribed useful bandwidth, in-band return loss, and out-of-band rejection, in complete analogy to a microwave filter. This goal is achieved by introducing between input and output the number of required resonators and appropriate coupling structures in order to achieve an electrically compliant response. Following this approach, the array design can be performed following, for instance, the filter design procedure described in [16]. Following this approach two different situations arise. The first is when the complete filter structure is inside the feeding waveguide, the second is when the filter structure is in the phase-shift wall waveguide.

The first design that we present consists of a two-pole structure inside the feeding waveguide [see Fig. 10(a)]. The frequency response of the structure is shown in Fig. 11. The angular variation of the frequency response (not shown here) appears to be largely invariant with respect to the angle of incidence.

The second structure that we present, again has two poles, but now they are implemented in the phase-shift wall wave-

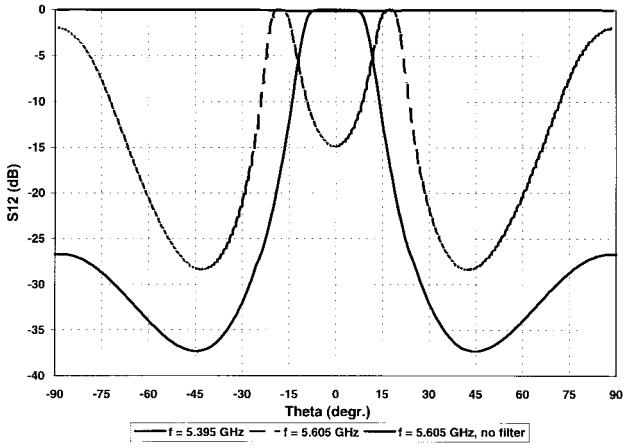

Fig. 12. H-plane angular response of the embedded element in the array antenna of Fig. 10(b) as function of frequency.

guide, as shown in Fig. 10(b) [17]. With this antenna we can get the same frequency response at broadside as with the previous antenna, but now the angular behavior depends on frequency. This is shown in Fig. 12 where we show the transmission pattern of an infinite array of square waveguides arranged in a rectangular grid. From this figure we see that when the frequency is increased, the antenna beam is launched at an angle with respect to the array normal, the angle increasing with frequency. The beam is invariant with the azimuth angle, so that "conical ring" antenna patterns are generated. The opening angle of the cone is controlled by the frequency. From the same figure we observe that by using this "space filter" for a fixed frequency, the angular element pattern can be significantly narrowed.

VI. Conclusions

A simple and efficient procedure for the study of infinite open-ended waveguide array antennas has been presented. A number of comparisons have been performed with both simulated and measured data thus fully validating the theoretical approach presented. In addition to theory, a novel phased-array antenna design procedure has been presented which can significantly increase the degrees of freedom in the electrical design.

Appendix
Phase-Shift Wall Waveguide Modes

Fig. 13 shows the phase-shift wall waveguide for an infinite array with a general triangular lattice. The key parameters are the distances s and t and the angle Ω (for $\Omega = \pi/2$, we have a rectangular lattice). For an empty waveguide with constant cross section under TM excitation, the vector mode functions $\mathbf{e}_{p,q}$ and $\mathbf{h}_{p,q}$ can be derived from the scalar-mode function $\phi_{p,q}(x, y)$ via [18]

$$\mathbf{e}_{p,q}(x, y) = -\frac{\nabla_t \phi_{p,q}(x, y)}{j\sqrt{k_{x_{p,q}}^2 + k_{y_{p,q}}^2}} \tag{A.1}$$

$$h_{p,q}(x, y) = \hat{z}_0 \times \mathbf{e}_{p,q}(x, y) \tag{A.2}$$

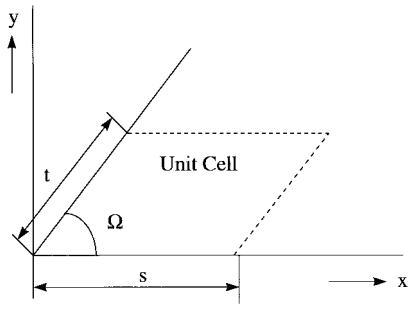

Fig. 13. General triangular lattice unit cell.

where $k_{x_{p,q}}$ and $k_{y_{p,q}}$ are the wave numbers in the transverse directions. The scalar-mode function $\phi_{p,q}(x, y)$ must satisfy the two-dimensional Helmholtz equation

$$(\nabla_t^2 + k_{x_{p,q}}^2 + k_{y_{p,q}}^2)\phi_{p,q} = 0 \tag{A.3}$$

together with the proper boundary conditions. Due to the periodic structure, the solution of (A.3) can be written in the form

$$\phi_{p,q}(x, y) = f(x, y)e^{-j(k_{x_0}x + k_{y_0}y)} \tag{A.4}$$

where

$$k_{x_0} = k_0 \sin(\vartheta)\cos(\varphi) \tag{A.5}$$

$$k_{y_0} = k_0 \sin(\vartheta)\sin(\varphi) \tag{A.6}$$

θ and φ being the angles with respect to the z and x axis, respectively, and

$$f(x + s, y) = f(x, y) \tag{A.7}$$

$$f(x + t\cos(\Omega), y + t\sin(\Omega)) = f(x, y). \tag{A.8}$$

Introducing (A.4)–(A.8) into (A.3), we obtain

$$\phi_{p,q}(x, y) = \frac{1}{\sqrt{st\sin(\Omega)}} \cdot e^{-j\{[k_{x_0} + (p2\pi/s)]x + [k_{y_0} - (p2\pi/s\tan(\Omega)) + (q2\pi/t\sin(\Omega))]y\}}. \tag{A.9}$$

Finally, for the TM vector-mode functions, we obtain

$$\mathbf{e}_{\mathrm{TM}_{p,q}}(x, y) = -\frac{1}{k_{T_{p,q}}}\frac{1}{\sqrt{st\sin(\Omega)}}(u_{p,0}\hat{x}_0 + v_{p,q}\hat{y}_0) \cdot e^{-j(u_{p,0}x + v_{p,q}y)} \tag{A.10}$$

$$\mathbf{h}_{\mathrm{TM}_{p,q}}(x, y) = -\frac{1}{k_{T_{p,q}}}\frac{1}{\sqrt{st\sin(\Omega)}}(-v_{p,q}\hat{x}_0 + u_{p,0}\hat{y}_0) \cdot e^{-j(u_{p,0}x + v_{p,q}y)} \tag{A.11}$$

where

$$k_{T_{p,q}} = \sqrt{u_{p,0}^2 + v_{p,q}^2} \tag{A.12}$$

$$u_{p,0} = k_0 \sin(\vartheta)\cos(\varphi) + \frac{p2\pi}{s} \tag{A.13}$$

$$v_{p,q} = k_0 \sin(\vartheta)\sin(\varphi) - \frac{p2\pi}{s\tan(\Omega)} + \frac{q2\pi}{t\sin(\Omega)}. \tag{A.14}$$

The derivation of the TE vector-mode functions follows the same procedure and, therefore, is not repeated.

ACKNOWLEDGMENT

The authors would like to thank S. Arons and F. Nennie for providing the array antenna measurements.

REFERENCES

[1] R. Mitrra and S. W. Lee, *Analytical Techniques in the Theory of Guided Waves.* New York: Macmillan, 1971, p. 19.
[2] V. Galindo and C. P. Wu, "Numerical solutions for an infinite phased array of rectangular waveguides with thick walls," *IEEE Trans. Antennas Propagat.*, vol. AP-14, pp. 149–158, Mar. 1966.
[3] A. Roederer, "Etude des Réseaux finis de Guides Rectangulaires à Parois Epaisses," *L'Onde Electrique*, vol. 51, fasc. 10, pp. 854–861, Nov. 1971 (in French).
[4] H. Patzelt and F. Arndt, "Double-plane steps in rectangular waveguides and their application for transformers, irises, and filters," *IEEE Trans. Microwave Theory Tech.*, vol. MTT-30, no. 5, pp. 771–776, May 1982.
[5] H. J. van Schaik, "The performance of an iris-loaded planar phased-array antenna of rectangular waveguides with an external dielectric sheet," *IEEE Trans. Antennas Propagat.*, vol. AP-26, pp. 413–419, May 1978.
[6] K. K. Chan and R. M. Turner, "Modal design of broadband wide-scan waveguide phased array," in *Int. Conf. Radar*, Paris, France, May 1994, pp. 707–712.
[7] K. K. Chan, H. J. Visser, W. P. M. N. Keizer, and R. M. Turner, "Dual polarized waveguide phased array for SAR application," in *Progress in Electromagn. Res. Symp.*, Noordwijk, The Netherlands, July 1994.
[8] Y. C. Shih, "The mode-matching method," *Numerical Techniques for Microwave and Millimeter-Wave Passive Structures*, T. Itoh, Ed. New York: Wiley, 1989.
[9] A. A. Melcon, G. Connor, and M. Guglielmi, "New simple procedure for the computation of the multimode admittance or impedance matrix of planar waveguide junctions," *IEEE Trans. Microwave Theory Tech.*, vol. 44, pp. 413–418, Mar. 1996.
[10] N. Marcuvitz, *Waveguide Handbook*. New York: McGraw-Hill, 1951.
[11] V. E. Boria, G. Gerini, and M. Guglielmi, "An efficient inversion technique for banded linear systems," in *IEEE MTT-S Int. Microwave Symp. Dig.*, Denver, CO, June 1997, pp. 1567–1570.
[12] V. E. Boria and M. Guglielmi, "Accelerated computation of admittance parameters for planar waveguide junctions," *Int. J. Microwave Millimeter-Wave*, vol. CAE-7, 1997.
[13] H. J. Visser and W. P. M. N. Keizer, "Waveguide phased array antenna analysis and synthesis," in *COST 245 Workshop Active Antennas*, Noordwijk, The Netherlands, June 1996, pp. 123–131.
[14] D. Kinowski and M. Guglielmi, "Multimode network representations for the scattering by an array of thick parallel plates," *IEEE Trans. Antennas Propagat.*, vol. 45, pp. 608–613, Apr. 1997.
[15] K. Kobayashi and K. Miura, "Diffraction of a plane wave by a thick grating," *IEEE Trans. Antennas Propagat.*, vol. 37, pp. 459–470, Apr. 1989.
[16] M. Guglielmi, "Simple CAD procedure for microwave filters and multiplexers," *IEEE Trans. Microwave Theory Tech.*, vol. 42, pp. 1347–1352, July 1994.
[17] D. Kinowski, M. Guglielmi, and A. G. Roederer, "Angular bandpass filters: An alternative viewpoint gives improved design flexibility," *IEEE Trans. Antennas Propagat.*, vol. 43, pp. 390–395, Apr. 1995.
[18] M. Guglielmi and A. A. Oliner, "Multimode network description of a planar periodic metal-strip grating at a dielectric interface—Part I: Rigorous network formulations," *IEEE Trans. Microwave Theory Tech.*, vol. 37, pp. 542–552, Mar. 1989.

Huib J. Visser (S'92–M'95) was born in Goes, The Netherlands, on October 26, 1964. He received the M.S. (electrical engineering) degree from Eindhoven University of Technology, The Netherlands, in 1989.

In 1990, after fulfilling his military service at TNO Physics and Electronics Laboratory, The Hague, The Netherlands, he joined the same laboratory as a civilian and now is a Principal Research Engineer in the Radar Department. He has participated in several projects concerning near-field antenna measurements, monolithic microwave integrated circuits design, and phased-array antenna design. From mid 1996 to mid 1997, he was stationed at the European Space Research and Technology Centre, RF Systems Division, Noordwijk, The Netherlands, where he worked on infinite waveguide array antenna modeling. His research interests are planar and conformal phased-array antennas and frequency selective surfaces.

Marco Guglielmi (SM'98) was born in Rome, Italy, on December 17, 1954. He received the "Laurea Ingegneria Elettronica" degree from the University of Rome "La Sapienza," Rome, Italy, in 1979, the M.S. (electrical engineering) degree from the University of Bridgeport, CT, in 1982, and the Ph.D. degree (electrophysics) from Polytechnic University, Brooklyn, NY, in 1986.

From 1984 to 1985, he was an Academic Associate at Polytechnic University and from 1986 to 1988 he was an Assistant Professor at the same university. From 1988 to 1989 he was an Assistant Professor at the New Jersey Institute of Technology, Newark, NJ. In 1989, he joined the RF System Division, European Space Research and Technology Centre, Noordwijk, The Netherlands, where he is currently involved in the development of passive microwave components for space applications. His professional interests include the areas of solid-state devices and circuits, periodic structures, phased arrays, and millimeter-wave leaky-wave antennas, network representations of waveguide discontinuities, and microwave filtering structures.

Dr. Guglielmi was awarded a Fulbright Scholarship in Rome, Italy, and an HISP scholarship (Halsey International Scholarship Program), from the University of Bridgeport, CT, in 1981.